Experimental Implementation of a Quantum Random-Walk Search Algorithm Using Strongly Dipolar Coupled Spins

Dawei Lu,[1] Jing Zhu,[1,2] Ping Zou,[3] Xinhua Peng,[1] Yihua Yu,[2]
Shanmin Zhang,[2] Qun Chen,[2] Dieter Suter,[4] and Jiangfeng Du[1,*]

[1]*Hefei National Laboratory for Physical Sciences at Microscale and Department of Modern Physics, University of Science and Technology of China, Hefei, Anhui, 230026, China*
[2]*Department of Physics & Shanghai Key Laboratory for Magnetic Resonance, East China Normal University Shanghai 200062*
[3]*Laboratory of Quantum Information Technology, ICMP and SPTE, South China Normal University, Guangzhou 510006, China*
[4]*Fakultät Physik, Technische Universität Dortmund, 44221 Dortmund, Germany*

An important quantum search algorithm based on the quantum random walk performs an oracle search on a database of N items with $O(\sqrt{N})$ calls, yielding a speed-up similar to the Grover's quantum search algorithm. The algorithm was implemented on a quantum information processor of three-qubit liquid-crystal nuclear magnetic resonance in the case of finding 1-out-of-4, and the diagonal elements' tomography of all the final density matrices was completed with comprehensible one-dimensional NMR spectra. The experimental results agree well with the theoretical predictions.

PACS numbers: 03.67.Lx, 05.40.Fb, 76.60.2k

I. Introduction

Quantum computation has attracted much attention for the past decade as quantum computers can efficiently solve problems which are intractable to classical computers. The computation tasks are rendered by algorithms. Since Shor's remarkable factoring algorithm [1], many quantum algorithms have been proposed. The algorithms presented early are mainly based on the quantum Fourier transform [1] and Grover's search algorithm [2]. Later two alternative trends have entered into the field, the adiabatic quantum algorithms [3] and quantum random walk [4–12]. In this paper, we focus on the quantum-walk based search algorithm.

Since the classical random walk is a useful tool for developing classical algorithms, the quantum random walk has been introduced as a potential method to formulate quantum algorithms. There are two distinct models, the continuous-time model and discrete-time model. The continuous-time model gives a unitary transformation directly in the space where the walk takes place. The discrete-time model requires an extra coin register and defines a two-step procedure consisting of a quantum coin flip followed by a coin-controlled walk step. Investigations show that quantum random walks have notable different features to their classical counterparts [4, 5]. These features may be used for designing quantum algorithms. Some relevant algorithms have been discovered with remarkable speedup over classical computation [8, 13]. The quantum search algorithm based on the quantum random walk proposed by Shenvi, Kempe, and Whaley (the SKW algorithm) [13] is one of the novel algorithms, for performing an oracle search on a database of N items with $O(\sqrt{N})$ calls, where N is the size of the search space. Despite of a similar speed-up to the Grover's quantum search algorithm, the SKW algorithm is important as there are situations when the diffusion step of Grover's algorithm can not be implemented efficiently. Various optimizations and improvements of the SKW algorithm have also been proposed in recent years [14–16, 18, 22], which can reduce the complexity and increase the search capability to a certain extent.

Some experiments about quantum random walk have been implemented in various physical systems under both continuous-time and discrete-time conditions [19–22], but as much as we know, no experiments about the algorithms based on quantum random walk have been reported. In this paper, we experimentally demonstrate the 1-out-of-4 case of the SKW algorithm [13] and show its superiority over classical algorithms. The experiments are performed on a quantum information processor of liquid-crystal nuclear magnetic resonance, with a strongly dipolar coupled Hamiltonian

$$\begin{aligned}\mathcal{H} = & \sum_j \pi\nu_j\sigma_z^j + \sum_{j<k}\frac{\pi}{2}J_{jk}\sigma_z^j\sigma_z^k \\ & + \sum_{j<k}\frac{\pi}{2}D_{jk}\left(2\sigma_z^j\sigma_z^k - \sigma_x^j\sigma_x^k - \sigma_y^j\sigma_y^k\right) \qquad (1)\end{aligned}$$

where ν_j is the resonance frequency of the jth spin, D_{jk} and J_{jk} are the dipolar coupling strengths and scalar coupling strengths between spins j and k, respectively. Here, weak J-couplings are assumed. The sums are restricted to the spins within one molecule. Since there exist non-diagonal elements in the Hamiltonian, the eigenstates are not Zeeman product states any more but linear combinations of them. We still utilize the spins to store information but to read information in the eigenbasis for more obvious and convenient tomography on NMR spectra. More details are described in Section III.

*Electronic address: djf@ustc.edu.cn

II. Algorithm

First we give an overview of the original algorithm. Consider the unstructured search problem: given a function $f(x)$, $f(x) = 1$ if $x = a$, otherwise $f(x) = 0$. The goal is to find a, where $0 \leqslant a \leqslant 2^n - 1$. It is equivalent to search for a single marked node among the $N = 2^n$ nodes on the n-cube.

The discrete-time random walk can be described by the repeated application of a unitary evolution operator U. U can be divided into two parts $U = SC$, where S is a permutation matrix which performs a controlled shift based on the state of the coin space, and C is a unitary matrix corresponding to "flipping" the quantum coin. To search for the node, SKW introduces an oracle whose function is determined by the coin operator. The oracle will act by applying a marking coin C_1 to the marked node and the original coin C_0 to the unmarked nodes. This new coin operator is named C'. Then the perturbed unitary evolution operator U' is given by $U' = SC'$ (see Fig.1). After applying U' for $t_f = \frac{\pi}{2}\sqrt{2^n}$ times, we will gain the marked state with probability $\frac{1}{2} - O(n)$ by measurement.

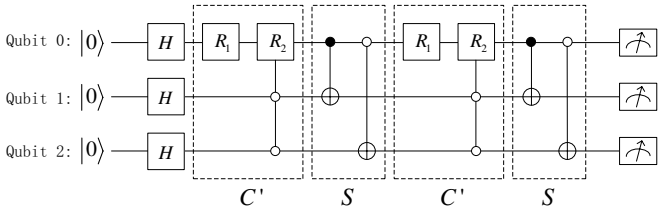

FIG. 1: Quantum network for the algorithm of 1-out-of-4 searching, with the target state being $|11\rangle_{13}$. The black dot represents 1-control gate while the white dot reversely. The purpose of C' is to implement $C_1 = R_x^2(\pi/2)$ (rotating qubit 2 around the x axis by angle $\pi/2$) when the "database" is $|11\rangle_{13}$ and $C_0 = R_x^2(3\pi/2)$ otherwise. It is equivalent to be replaced by $R_1 = R_x^2(3\pi/2)$ and $R_2 = R_x^2(-\pi)$. The two controlled-not gates are inverting qubit 1 if qubit 2 is $|1\rangle_2$ and inverting qubit 3 if qubit 2 is $|0\rangle_2$, respectively. The measurement is all the populations', namely, diagonal elements' reconstruction. Similar circuits can be obtained straightforwardly for other target states. For instance if the goal is $|10\rangle_{13}$, we need only change the controlled condition of the three-body-interaction gate to state $|10\rangle_{13}$.

When $n = 2$, three qubits are needed to demonstrate the algorithm. One qubit is used as the "coin" (referred as the "coin qubit", labeled by qubit 2), while the other two are used as the database (referred as the "database qubits", labeled by qubit 1 and 3). The target state is $|\tau\sigma\rangle_{13} = |\tau\rangle_1 \otimes |\sigma\rangle_3 (\tau, \sigma = 0, 1)$ out of the four computational basis $|00\rangle_{13}, |01\rangle_{13}, |10\rangle_{13}, |11\rangle_{13}$. The 1-out-of-4 algorithm is implemented as the network shown in Fig.1. Without losing generality, suppose the initial state is $|111\rangle$.

(i) Prepare the state

$$|\psi_i\rangle = \frac{|0\rangle_1 - |1\rangle_1}{\sqrt{2}} \otimes \frac{|0\rangle_2 - |1\rangle_2}{\sqrt{2}} \otimes \frac{|0\rangle_3 - |1\rangle_3}{\sqrt{2}}, \qquad (2)$$

which is exactly an equal superposition over all the computational basis. It is simple to do this by applying a Hadamard operation to every qubit.

(ii) On each step, the "coin qubit" undergose a unitary operation depending on the state of "database qubits", namely, $C_1 = R_x^2(\pi/2) = e^{-i\pi\sigma_x/4}$ if the "database qubits" are on the target state $|\tau\sigma\rangle_{13}$, and $C_0 = R_x^2(3\pi/2) = e^{-i3\pi\sigma_x/4}$ otherwise (In Fig.1, this controlled operation is simplified through $R_1 = R_x^2(3\pi/2) = e^{-i3\pi\sigma_x/4}$ and $R_2 = R_x^2(-\pi) = e^{i\pi\sigma_x/2}$ equivalently). Therefore the whole "coin" operation is

$$C' = C_0 \otimes E_{13} + (C_1 - C_0) \otimes |\tau\sigma\rangle_{1313} \langle\tau\sigma| \qquad (3)$$

where E_{13} is the identity operator on the "database qubits". Then the "database qubits" undergo the shift operation S conditioned on the state of "coin qubit":

$$\begin{aligned} |0\rangle_2 |00\rangle_{13} &\Longleftrightarrow |0\rangle_2 |01\rangle_{13} \\ |0\rangle_2 |10\rangle_{13} &\Longleftrightarrow |0\rangle_2 |11\rangle_{13} \\ |1\rangle_2 |00\rangle_{13} &\Longleftrightarrow |1\rangle_2 |01\rangle_{13} \\ |1\rangle_2 |01\rangle_{13} &\Longleftrightarrow |1\rangle_2 |11\rangle_{13} \end{aligned} \qquad (4)$$

(iii) After repeating step (ii) twice, it reaches the final state

$$|\psi_f\rangle = (SC')^2 |\psi_i\rangle \qquad (5)$$

For example, in the case of finding $|11\rangle_{13}$, $|\psi_f\rangle$ is specialized as

$$|\psi_f\rangle = \frac{\sqrt{2}}{4}|001\rangle + \frac{\sqrt{2}}{4}|101\rangle + \frac{\sqrt{2}}{4}|010\rangle + \frac{\sqrt{2}}{4}|110\rangle + \frac{\sqrt{2}}{2}|011\rangle \qquad (6)$$

Through this expression we can obtain that the theoretic probabilities of $|00\rangle_{13}, |01\rangle_{13}, |10\rangle_{13}, |11\rangle_{13}$ are 0, 0.25, 0.25, 0.5 respectively after tracing qubit 2 out.

For other target states, similar circuits can be given easily with the controlled condition changed. The theoretic results have an analogy with the above.

III. Implementation

A. System

To implement the algorithm we used the three ^1H spins in a sample of 1-Bromo-2,3-Dichlorobenzene oriented in liquid-crystal solvent ZLI-1132. All experiments were conducted on a Bruker Avance 500 MHz spectrometer at room temperature. The molecular structure is shown in Fig.2(a). The internal Hamiltonian of this system can be described as

$$\begin{aligned} \mathcal{H} = & \sum_{j=1}^{3} \pi\nu_j\sigma_z^j + \sum_{j,k,j<k\leqslant 3} \frac{\pi}{2} J_{jk}\sigma_z^j\sigma_z^k \\ & + \sum_{j,k,j<k\leqslant 3} \frac{\pi}{2} D_{jk}\left(2\sigma_z^j\sigma_z^k - \sigma_x^j\sigma_x^k - \sigma_y^j\sigma_y^k\right) \end{aligned} \qquad (7)$$

The spectrum of the thermal equilibrium state $\rho_{th} = \sum_{i=1}^{3} \sigma_z^i$ followed by a $\pi/2$ hard pulse is shown in Fig.2(b). With some initially guessed parameters (chemical shifts, scalar coupling constants and dipolar coupling constants), we iteratively fit the calculated and observed spectra through the parameters' perturbation. All the calculated values are listed in Tab. Ia.

(a)

	H_1	H_2	H_3
H_1	1945.5	−1633.3	−1341.7
H_2	8	2094.8	−339.35
H_3	8	1.4	2147.2

(b)

spin 1 No.9	$UR_y^1(\pi/2)$	$UR_y^1(\pi/2)R_y^2(\pi)$	$UR_y^1(\pi/2)R_y^3(\pi)$	$UR_y^1(\pi/2)R_y^{2,3}(\pi)$
	$P(1)-P(5)$	$P(3)-P(7)$	$P(2)-P(6)$	$P(4)-P(8)$
spin 2 No.8	$UR_y^2(\pi/2)$	$UR_y^2(\pi/2)R_y^1(\pi)$	$UR_y^2(\pi/2)R_y^3(\pi)$	$UR_y^2(\pi/2)R_y^{1,3}(\pi)$
	$P(2)-P(4)$	$P(6)-P(8)$	$P(1)-P(3)$	$P(5)-P(7)$
spin 3 No.7	$UR_y^3(\pi/2)$	$UR_y^3(\pi/2)R_y^1(\pi)$	$UR_y^3(\pi/2)R_y^2(\pi)$	$UR_y^3(\pi/2)R_y^{1,2}(\pi)$
	$P(1)-P(2)$	$P(5)-P(6)$	$P(3)-P(4)$	$P(7)-P(8)$

TABLE I: (a) The Hamiltonians of 1-Bromo-2,3-Dichlorobenzene. The diagonal elements are chemical shifts of the three protons, the upper-right off-diagonal elements are dipolar coupling strengths while the lower-left are scalar coupling strengths. (b) The read-out pulses and corresponding values of $P(i) - P(j)$. The results are showed on the transitions of No.9, 8 and 7. Combined with the normalized condition $\sum_{i=1}^{8} P(i) = 1$, all the diagonal elements can be solved.

With the system Hamiltonian confirmed, we consider the procedure of diagonalizing the Hamiltonian. It is not difficult to find a feasible unitary matrix U to equalize

$$H_L = U H_S U^\dagger \tag{8}$$

where H_S is the system Hamiltonian and H_L is a diagonal Hamiltonian, i.e., an Ising type Hamiltonian. Specially, for the system Hamiltonian mentioned above, the transformation U we have selected is

$$\begin{pmatrix} 1 & 0 & 0 & 0 & 0 & 0 & 0 & 0 \\ 0 & 0.801 & 0.512 & 0 & -0.303 & 0 & 0 & 0 \\ 0 & 0.375 & -0.823 & 0 & -0.420 & 0 & 0 & 0 \\ 0 & 0 & 0 & 0.810 & 0 & 0.126 & 0.559 & 0 \\ 0 & -0.467 & 0.223 & 0 & -0.856 & 0 & 0 & 0 \\ 0 & 0 & 0 & 0.458 & 0 & -0.730 & -0.508 & 0 \\ 0 & 0 & 0 & 0.344 & 0 & 0.672 & -0.656 & 0 \\ 0 & 0 & 0 & 0 & 0 & 0 & 0 & 1 \end{pmatrix}$$

which is one feasible unitary matrices that can diagonalize the Hamiltonian. Through this labeling scheme all the transitions are between two eigenstates from $|000\rangle_L$ to $|111\rangle_L$ with $|000\rangle_L = |000\rangle_S, |111\rangle_L = |111\rangle_S$, where the subscripts L and S represent the H_L and H_S picture. The nine observable transitions in the thermal equilibrium spectrum are marked in the transition diagram (Fig.2(c)).

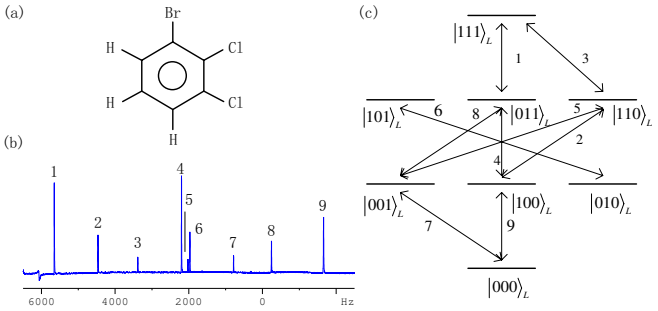

FIG. 2: (Color online)(a) The molecular structure of 1-Bromo-2,3-Dichlorobenzene with the three protons forming 3-qubit system. (b) The spectrum of the thermal equilibrium state $\rho_{th} = \sum_{i=1}^{3} \sigma_z^i$ followed by a $\pi/2$ hard pulse. All the transitions are labeled according to the descending orders of the frequencies. (c) The diagram of corresponding transitions in the H_L picture. No.1 and No.9, No.2 and No.8, and No.3 and No.7 lines express the transitions of qubit 1, 2 and 3 in the H_L picture, respectively.

Without loss of generality, we focused on the right three transitions No.7, 8 and 9, which cover all the three qubits' single-quantum transitions. Considering a simple case that ρ_S is a pure state $(|000\rangle\langle 000|)_S$. In the Ising model, if the transition of qubit 1 is excited (a selective pulse $R_y^1(\pi/2)$ is enough), a single peak can be obtained in the spectrum. This is a universal way to test the created pseudo pure state in liquid state NMR. However, in the current Heisenberg model, since the Hamiltonian's noncommunity, a single qubit rotation will not lead to a single peak but combination of some relative peaks (see the right column of Fig.3). The complicated spectrum is obviously not convenient to read out the information of density matrix. A straight idea to solve the problem is to utilize the H_L picture where the Hamiltonian is an Ising type. From Eq.8 we can clearly see that adding the transformation matrix U before the read-out pulse is all right. The right column of Fig.3 shows the spectra of $(|000\rangle\langle 000|)_S$ with three read-out pulses $UR_1^y(\pi/2), UR_2^y(\pi/2)R_3^y(\pi), UR_3^y(\pi/2)$. The second pulse needs a $R_3^y(\pi)$ rotation as transition No.8 represents $|001\rangle_L \rightarrow |011\rangle_L$, not $|000\rangle_L \rightarrow |010\rangle_L$. The simulating spectra accord well with the expected results, similarly to the Ising type.

For reading-out the diagonal elements of a general density matrix ρ_S, the method above is still effective. Defining the populations of $(|000\rangle\langle 000|)_S$ to $(|111\rangle\langle 111|)_S$ are $P(1)$ to $P(8)$, $UR_1^y(\pi/2)$ would excite the transitions $|000\rangle_L \rightarrow |100\rangle_L$ and $|100\rangle_L \rightarrow |000\rangle_L$, displayed on transition No.9. Compared with the integration of the pure-state case, we can obtain the value of $P(1)-P(5)$. Table. I (b) shows all the available values of $P(i)-P(j)$ through different read-out pulses. Combined with the normalization condition $\sum_{i=1}^{8} P(i) = 1$, all the eight population values can be calculated. Now we have accomplished the diagonal elements' tomography.

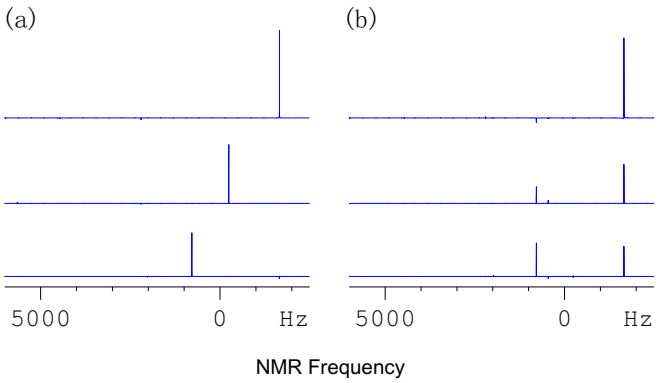

FIG. 3: (Color online) Simulation of the PPS's observation. The left column (a) shows the spectra with the read-out pulses $UR_1^y(\pi/2), UR_2^y(\pi/2)R_3^y(\pi), UR_3^y(\pi/2)$, while the right (b) shows the spectra with the traditional read-out pulses $R_1^y(\pi/2), R_2^y(\pi/2), R_3^y(\pi/2)$. We can see that the spectra (a) are more comprehensible than that of (b).

B. Experiment

The experiment was divided into three steps: the psesudo-pure state preparation, quantum random walk searching process, and populations' measurement. Starting from the thermal equilibrium state, firstly we need to create the PPS $\rho_{000} = \frac{1-\epsilon}{8}\mathbf{1} + \epsilon\,|000\rangle\langle 000|$, where ϵ represents the polarization of the system and $\mathbf{1}$ is the identity matrix. We used strongly modulating pulses based on GRadient Ascent Pulse Engineering (GRAPE) algorithm [23] and gradient pulses to realize the PPS preparation, with the numerical simulated fidelity 97.7%. The top spectrum of Fig. 4 (a) shows the experimental observation of the PPS about the first qubit in H_L picture, which exhibits a single absorption-shape peak if discarding the small errors.

The quantum random walk searching process contains two parts actually: The preparation of initial state $|-\rangle^{\otimes 3}$ ($|-\rangle = (|0\rangle - |1\rangle)/\sqrt{2}$) and two times of unitary evolution. We packed them together and calculated one GRAPE pulse of 20ms and 250 segments whose fidelity is higher than 0.99 to realize it. The reading-out operators listed in Table. I (b) are also performed when generating the GRAPE pulses of 20ms with the fidelity 0.99. Four spectra observed on transition No.9 are shown in Fig. 4 (a). The calculated populations according to the experimental data are shown in Fig. 4 (b). The fidelity of the diagonal elements of the final density matrix is 0.983, with the probabilities of gaining $|00\rangle_{13}$, $|01\rangle_{13}$, $|10\rangle_{13}$, $|11\rangle_{13}$ being 0.513, 0.232, 0.197, 0.058. It demonstrates that we have completed searching $|00\rangle_{13}$ based on the SKW algorithm.

Besides $|00\rangle_{13}$, we altered the target states to $|01\rangle_{13}$, $|10\rangle_{13}$ and $|11\rangle_{13}$. The experimental results after the SKW algorithm are exhibited in Fig. 5. It can be seen the experimental and theoretical results are mostly consistent with little error. The slight difference between theory and experiment may be attributed to decoherence, the RF field inhomogeneity and imperfections of GRAPE pulses.

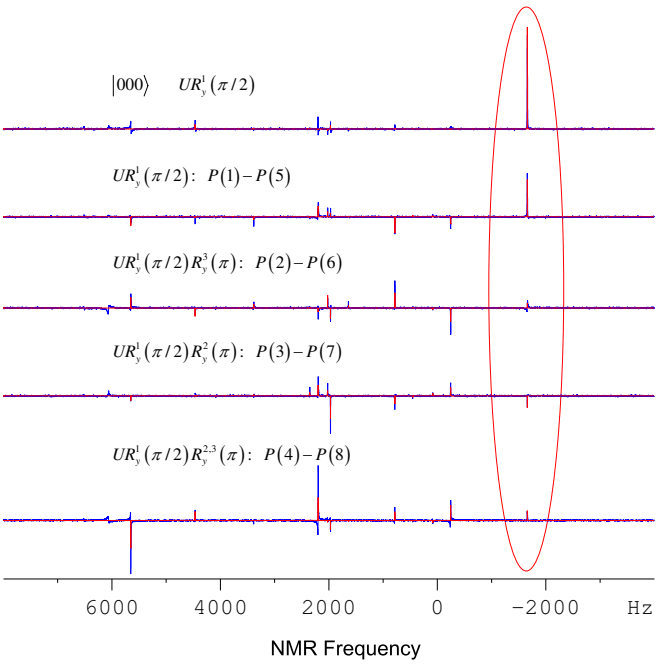

FIG. 4: (Color online)(a) One-dimensional NMR spectra for measuring the diagonal elements (first qubit) of H_L. As shown in Table. I (b), we just concentrate on transition No.9 (marked by the ellipse) to read out $P(1)-P(5)$, $P(2)-P(6)$, $P(3)-P(7)$ and $P(4)-P(8)$, with the four operators listed in the figure. The top spectrum is the observation of the PPS $|000\rangle$, which is usd as the benchmark. The theoretical values of the four population-subtractions are 0.375, 0, -0.125, 0.125, while the experimental results are 0.383, 0.050, -0.061, 0.093. (b) The calculated populations according to the experimental data. The blue columns are theoretical results and the red columns are experimental results. The fidelity is 0.983.

IV. Conclusion

In summary, we experimentally implemented the search algorithm based on the quantum random walk (the SKW algorithm) in the case of 1-out-of-4. This algorithm performs an oracle search on a database of N items with $O(\sqrt{N})$ calls, having a speed-up similar to the Grover's search algorithm. The experiment was carried out on an NMR spectrometer with strongly dipolar coupled spins. The process of diagonalization of the spin Hamiltonian was executed in a program written by MATLAB. We used GRAPE pulses to realize high-fidelity coherent control and provided an effective way to measure the diagonal elements of the density matrix with one-dimensional NMR spectra. This method can be extended to full tomography and higher qubits. For strong J-coupling strengths it is also effective. The experimental results match well with the theoretical expectations, which exhibit the superiority of the algorithm.

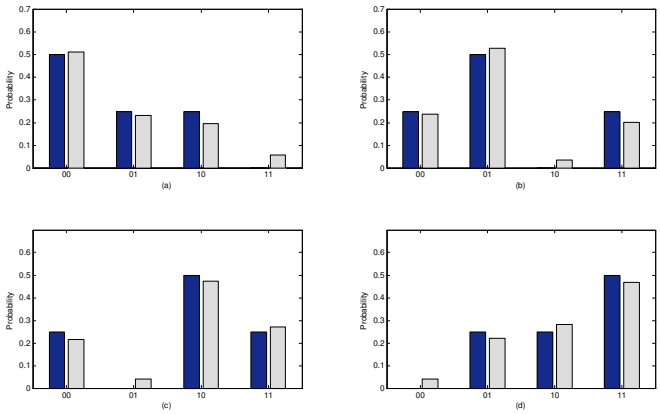

FIG. 5: (Color online)The comparison between the theoretical predictions and experimental results after implementing the SKW algorithm. (a), (b), (c), (d) correspond to the cases of finding $|00\rangle_{13}$, $|01\rangle_{13}$, $|10\rangle_{13}$ and $|11\rangle_{13}$. The blue bars represent the theoretical prediction while the red bars represent the experimental analogue.

Acknowledgement

We thank Yiheng Lin, Hongwei Chen, Nanyang Xu, Peng Li, Ya Wang and Zhaokai Li for helpful discussions. This work was supported by National Nature Science Foundation of China, the CAS, Ministry of Education of RPC, the National Fundamental Research Program, and the DFG through Su 192/19-1.

[1] P. W. Shor, SIAM J. Comput. **26**, 1484 (1997).
[2] L. Grover,Phys. Rev. Lett. **79**, 325 (1997).
[3] Farhi E, Goldstone J, Gutmann S, Lapan J, Lundgren A, and Preda D, Science **292**,412 (2001).
[4] Y. Aharonov, L. Davidovich, and N. Zagury, Phys. Rev. A **48**, 1687 (1993).
[5] E. Farhi and S. Gutmann, Phys. Rev. A **58**, 915 (1998).
[6] A. Ambainis, E. Back, A. Nayak, A. Vishwanath, and J. Watrous, in *Proceedings of the 30th annual ACM Symposium on Theory of Computing* (Association for Computing Machinery, New York, 2001), pp. 60-69.
[7] A. Childs, E. Farhi, and S. Gutmann, Quantum Inform. Process. **1**, 35 (2002).
[8] A. Childs, R. Cleve, E. Deotto, E. Farhi, S. Gutmann, and D. Spielman, Proc. 35th ACM Symposium on Theory of Computing (STOC 2003), pp. 59-68.
[9] T. A. Brun, H. A. Carteret and A. Ambainis, Phys. Rev. Lett. **91**, 130602 (2003).
[10] A. Ambainis, SIAM J. Comput. **37**, 210 (2007).
[11] E. Farhi, J. Goldstone, and S. Gutmann, Theory Comput. **4**, 169 (2008).
[12] A. Childs, Phys. Rev. Lett. **102**, 180501 (2008).
[13] N. Shenvi, J. Kempe and K. B. Whaley, Phys. Rev. A **67**, 052307 (2003).
[14] A. Ambainis, J. Kempe, and A. Rivosh, *Proceedings of the 16th ACM-SIAM SODA* (Society for Industrial and Applied Mathematics, Philadelphia, 2005), pp. 1099C1108.
[15] A. Tulsi, Phys. Rev. A **78**, 012310 (2008).
[16] D. Reitzner, M. Hillery, E. Feldman, and V. Bužek, Phys. Rev. A **79**, 012323 (2009).
[17] C. M. Chandrashekar, R. Srikanth, and R. Laflamme, Phys. Rev. A **77**, 032326 (2008).
[18] V. Potoček, A. Gábris, T. Kiss and I. Jex, Phys. Rev. A **79**, 012325 (2009).
[19] B. C. Travaglione and G. J. Milburn, Phys. Rev. A **65**, 032310 (2002).
[20] J. Du et al., Phys. Rev. A **67**, 042316 (2003).
[21] C. A. Ryan, M. Laforest, J. C. Boileau, and R. Laflamme, Phys. Rev. A **72**, 062317 (2005).
[22] C. M. Chandrashekar, Phys. Rev. A **74**, 032307 (2006).
[23] J. Baugh et al., Phys. in Can. **63**, No.4 (2007), 'Special issue on quntum information and quantum computing'; N. Khaneja et al., J. Magn. Reson. **172**, 296 (2005); C. A. Ryan et al., Phys. Rev. A **78**, 012328 (2008).